

Influence of electronic entropy on Hellmann-Feynman forces in *ab initio* molecular dynamics with large temperature changes

Ming Geng (耿明) ^{1,2} and Chris E. Mohn^{1,2,3,*}

¹Centre for Planetary Habitability (PHAB), University of Oslo, N-0315 Oslo, Norway

²Centre for Earth Evolution and Dynamics (CEED), University of Oslo, N-0315 Oslo, Norway

³Department of Chemistry and Center for Materials Science and Nanotechnology, University of Oslo, Oslo 0371, Norway



(Received 7 August 2023; revised 20 September 2023; accepted 22 September 2023; published 19 October 2023)

The Z method is a popular atomistic simulation method for determining the melting temperature where a sequence of microcanonical molecular dynamics runs are carried out to target the lowest system energy where the solid always melts. Homogeneous melting at the limit of critical superheating T_h is accompanied by a drop in temperature as kinetic energy is converted to potential energy and the equilibrium melting temperature T_m can be calculated directly from the liquid state. Implementation of the Z method interfaced with modern *ab initio* electronic structure packages often use Hellmann-Feynman forces to propagate the ions in the microcanonical ensemble where the Mermin free energy plus the ionic kinetic energy is conserved. The electronic temperature T_{el} is therefore *kept fixed* along the trajectory which may introduce some spurious ion-electron interactions in molecular dynamics runs with large changes in temperatures such as often seen in homogeneous melting and freezing processes in the microcanonical ensemble. We estimate possible systematic errors in the calculated melting temperature to choice of T_{el} for two main mantle components: the insulators SiO_2 and CaSiO_3 at high pressure. Comparison of the calculated melting temperature from runs where $T_{el} = T_h$ and $T_{el} = T_m$, representing reasonable upper and lower boundaries, respectively, to choice of T_{el} , shows that the difference in melting temperature is 200–300 K (3%–5% of the melting temperature) for our two test systems. Our results are in good agreement with previous large-size coexistence method and thermodynamic integration calculations, suggesting that CaSiO_3 and SiO_2 melt at around 6500 K (100 GPa) and 6000 K (160 GPa), respectively. The melting temperature decreases with increasing T_{el} due to the increasing entropic stabilization of the liquid and the systems melt typically about three times faster in molecular dynamics runs with $T_{el} = T_h$ compared to runs where $T_{el} = T_m$. A careful choice of electron temperature in Born-Oppenheimer molecular dynamics simulations where the ions are propagated using Hellmann-Feynman forces with the Mermin free energy + the ionic kinetic energy being conserved is therefore essential for the critical evaluation of the Z method and, in particular, at very high temperatures.

DOI: [10.1103/PhysRevB.108.134110](https://doi.org/10.1103/PhysRevB.108.134110)

I. INTRODUCTION

Melting and solidification processes are ubiquitous in condensed matter physics and in the evolution of terrestrial bodies including our own Earth. Triggered by extended defects, grain boundaries, or open surfaces, equilibrium melting occurs spontaneously at T_m when the free energy of the solid equals that of the liquid. Under certain conditions, however, a crystal can melt *homogeneously* at a much higher temperature T_h , which represents the critical limit of superheating before melting is unavoidable [1,2]. If a perfect periodic crystal in a molecular dynamics simulation is heated until $T \approx T_h$, spontaneous fluctuations (nucleation precursors) will form transient defects and liquid nuclei which trigger an irreversible rapid nucleation growth and melting. Although homogeneous melting is rare in nature, shock-induced homogeneous melting has been demonstrated in a number of experiments (see, for example, [3–8]).

The Z method explores the link between homogeneous and equilibrium melting using molecular dynamics simulations and has been widely used to estimate melting temperatures for different materials [9–13] often at high temperatures and pressure where experiments are hazardous or impractical [14–19]. A number of molecular dynamics simulations are launched in the microcanonical (NVE) ensemble at different initial temperatures T_{mi} to target the lowest total energy E_h , where the solid always melts. When the system melts at E_h (T_h), the temperature decreases to the equilibrium melting temperature while the latent heat of melting gradually converts into potential energy. If we assume a linear variation of energy with temperature we can establish a relationship between T_h and T_m from the entropy of melting [1,20]:

$$\frac{T_h}{T_m} - 1 = \frac{\Delta S_m}{C_V}, \quad (1)$$

where C_V is the heat capacity at constant volume of the solid and ΔS_m is the entropy of melting. Equation (1) can be approximated by $(\ln 2)/3$ assuming an ideal entropy of melting [$\ln 2k_B$ (per atom)] taken from a high-temperature limit of the

*chris.mohn@kjemi.uio.no

Debye model and assuming that the heat capacity at constant volume is given by $3k_B$ (per atom) when $\Delta V_m/V \rightarrow 0$ [21].

Since the equilibrium melting temperature can be calculated from a homogeneous melting process triggered typically by small defects, quite small simulation boxes (~ 100 atoms) are in general sufficient to accurately calculate T_h and hence T_m from Eq. (1) [22]. The use of small simulation boxes therefore makes the Z method a potentially attractive “low-cost” method for the accurate calculation of melting temperatures [22–24]. By contrast, popular two-phase approaches to melting where the equilibrium melting process is mimicked by constructing a simulation box with a solid and a liquid phase in mechanical contact, often require large boxes to accommodate both solid and liquid phases as well as their interfaces [25,26].

In addition, since T_m can be calculated from Eq. (1), there is no need for the explicit calculation of free energies which sometimes hamper the precision of thermodynamic integration [27,28] and two-phase thermodynamics (2PT) methods [29], especially when the solid and liquid free-energy curves have very similar steepness near T_m [25,30].

In spite of these advantages, recent studies have unveiled some artificial features that may hamper the Z method for the accurate calculation of melting temperatures, particularly under extreme conditions [23,25,31,32]. Since the waiting time required for the solid to melt diverges in the limit where $T_{ini} \rightarrow T_h$, a waiting-time analysis is often carried out at different $T_{ini} > T_h$ to estimate T_m from an extrapolation to that of “infinite” waiting time [23]. This analysis, however, may still require extensive statistics for the precise calculation of melting temperatures.

Moreover, Born-Oppenheimer *ab initio* molecular dynamics (BOMD) is typically performed in the NVE ensemble using Hellman-Feynman dynamics where the Fermi-Dirac electronic temperature is *kept fixed* in the MD simulation [33]. Although this implementation of the Z method ensures conserved dynamics [34,35], large changes in temperature following melting and sometimes equilibration may introduce systematic errors in T_m since the electronic temperature is kept fixed [25]. That is, if a BOMD NVE run with $E > E_h$ is launched with an T_{el} *chosen near the liquid temperature* ($T_{el} \approx T_m$), then T_{el} will be much lower than the temperature in the solid state (before melting). A too low electronic entropy may favor the stabilization of the solid and prevent melting. This in turn will affect the estimated homogeneous melting temperature (T_h) and the “waiting time” for a solid to melt. The calculated equilibrium melting temperature may therefore be too high. On the other hand, if a BOMD run is launched with an electronic temperature *chosen near the solid temperature before melting* ($T_{el} \approx T_h$), a physically reasonable electronic-ionic interaction is ensured before melting. However, once the solid melts at constant volume, the temperature drops by $1 - T_m/T_h \approx (\ln 2)/3$ and the electronic entropy will be much *higher* than the liquid temperature, which usually favors an entropic stabilization of the liquid. Hence, the melting temperature may be too low. Therefore, since the choice of electronic entropy affects Hellman-Feynman dynamics in processes undergoing large temperature drops, such as melting in the microcanonical ensemble, addressing the sensitivity in T_m to the choice of T_{el} is crucial in order to bench-

mark the Z method for the accurate calculating of melting temperatures.

In this work, we thus investigate the role of electronic entropy on homogeneous melting using Hellman-Feynman forces to propagate the ions for two main abundant mineral components in the Earth’s interior: CaSiO_3 and SiO_2 at high temperatures.

Ca-perovskite is the third most abundant mineral in the lower mantle and a main component of basaltic lithologies constituting more than 20% of recycled oceanic crust that is continuously being injected into the Earth’s deep interior. A strong preferential partitioning of radioactive heat-producing elements into CaSiO_3 , such as U and Th, as well as key geochemical tracers, suggests that CaSiO_3 is the main storage mineral for many of these minority elements [36,37]. Tracking the distribution of CaSiO_3 in the lowermost mantle is therefore essential to understand the evolution of the solid Earth, which in turn requires the thermodynamic conditions of Ca-perovskite melting. Motivated by this, a number of computational studies have calculated melting curves for pure CaSiO_3 to lowermost mantle conditions [20,25], but the agreement is not satisfactory. Here we attempt to contribute to tighten the constraints of CaSiO_3 melting at the lowermost mantle conditions.

Our second model system is SiO_2 . The solid-liquid phase boundary of SiO_2 at ultrahigh pressure is critical to our understanding of not only the Earth’s evolution but also the formation of many super Earths [38,39]. High-pressure silica melting may also play an important role in core dynamics, as it has been suggested that silica may have crystallized from a Si-saturated protocore during a chemical exchange with a basal magma ocean [40,41]. In spite of a number of simulations and experimental results reported in the literature, the SiO_2 melting curve remains poorly constrained at very high pressure. Here we will attempt to contribute to resolving some of these outstanding discrepancies.

II. THEORY

The thermodynamic ensemble appropriate for the Z method is the NVE ensemble with the volume V , number of species N , and the system energy E kept fixed. The maximum energy along the solid branch of the isochore E_h is the same as the lowest energy along the liquid branch:

$$E_{\text{sol}}(V, T_h) = E_{\text{liq}}(V, T_m). \quad (2)$$

To locate $E_{\text{sol}}(V, T_h)$ and hence $E_{\text{liq}}(V, T_m)$, a sequence of NVE MD runs are carried out with different initial temperatures. Since the waiting time for the solid to melt diverges when $T \rightarrow T_h$, the calculated melting temperature will always represent an upper bound to the “true” melting temperature. To avoid extremely long MD runs in the vicinity of T_h , the melting temperature is calculated from an extrapolation of the distributions of waiting times using

$$\langle \tau \rangle^{-1/2} = A(T_{\text{liq}} - T_m), \quad (3)$$

where “A” is a parameter, τ is the waiting time for a solid to melt at a given total energy, and T_{liq} is the liquid temperature of the system after melting. Since $T_{\text{liq}} = T_m$, when $E = E_h$, the melting temperature can be found at infinite waiting time, i.e., at the point of intersection where $\langle \tau \rangle^{-1/2} = 0$.

We use *ab initio* Born-Oppenheimer MD to propagate the ions where the electronic energy is minimized at each step along the trajectory. Note that the usual Hellmann-Feynman force does not conserve the total system energy $E = U + K$ where U is the internal DFT energy and K is the kinetic energy of the ions. This is because the energy functional is nonvariational with respect to changes in partial orbital occupancies along the MD trajectory, when the ions are propagated using the Hellmann-Feynman forces. The force, \mathbf{F} , that conserves the total energy is given as [34]

$$\mathbf{F} = \mathbf{F}^{\text{HF}} - \sum_i \frac{\delta U}{\delta f_i} \frac{\delta f_i}{\delta(\epsilon_i - E_F)} \nabla(\epsilon_i - E_F), \quad (4)$$

where \mathbf{F}^{HF} is the exact Hellmann-Feynman force (including possible contributions from Pulay stress). E_F is the Fermi level whereas ϵ_i and f_i are the eigenvalues and the electron occupancy of band i .

To avoid additional contributions to the Hellmann-Feynman forces due to the variation in the band occupancies along the ionic trajectory one can enforce a new conservation law where the quantity “ $K + \Omega$ ”, rather than “ $U + K$ ”, is conserved in the MD run where Ω is the Mermin free energy [34,35,42,43]

$$\Omega = U - T_{\text{el}} S_{\text{el}} \quad (5)$$

with

$$S_{\text{el}} = -k_B \sum_i [f_i \ln f_i + (1 - f_i) \ln(1 - f_i)]. \quad (6)$$

S_{el} is the electronic entropy and f_i is calculated using Fermi-Dirac statistics:

$$f_i = F\left(\frac{\epsilon_i - E_F}{\sigma}\right), \quad \sum_0^{N_i} f_i = N, \quad (7)$$

where F is the usual (Fermi-Dirac) smearing function, and $\sigma = k_B/T$ is the smearing broadening.

Ionic dynamics may be sensitive to the choice of electronic temperature when the ions are propagated using Hellmann-Feynman forces, in particular when the temperature changes are large such as during equilibration and melting in the NVE ensemble. Electronic temperature may therefore affect the melting processes for semiconductors and insulators even though the fractional occupancies of the conduction bands remain small during these temperature changes.

We can estimate the sensitivity in the calculated T_m to choices of T_{el} by comparison of the melting temperature calculated using $T_{\text{el}} \approx T_h$ with that calculated using $T_{\text{el}} \approx T_m$. These choices of T_{el} provide reasonable upper and lower bounds to the calculated melting temperature in the microcanonical ensemble when the Hellmann-Feynman forces are used for the ionic propagation with $K + \Omega$ being conserved.

If changes in T_{el} cannot be ignored, the usual conservation law including the Mermin functional in the form of Eq. (5) must be replaced, but the forces will then include contributions arising due to changes in the partial orbital occupancies along the microcanonical Born-Oppenheimer trajectory. It is important to note, however, that the time evolution of orbital occupancies due to large temperature changes may be only correctly described by the time-dependent Schrödinger equation [44].

A possible strategy to calculate T_m using the Z method is to adjust T_{el} along the ionic trajectory to match the average (ionic) temperature in the previous N time steps [25]. Although this “update scheme” does not ensure conserved dynamics, difference in the average ensemble temperature before and after the adjustment is in general expected to be small. In this approach, the time-dependent Schrödinger equation is thus approximated by a sequence of BOMD NVE simulations.

III. COMPUTATIONAL DETAILS

All BOMD simulations are performed with the Vienna *ab initio* simulation package (VASP) [45–48], using the projector augmented wave (PAW) method [49,50]. We use the generalized gradient approximation (GGA) where the exchange-correlation contribution to the energy is parametrized using the Perdew-Burke-Ernzerhof (PBE) [51] functional for SiO_2 and the Armiento and Mattsson 2005 (AM05) functional [52] for CaSiO_3 . The electronic configurations were $[\text{He}]2s^2 2p^4$ for O, $[\text{Ne}]3s^2 3p^2$ for Si, and $[\text{He}]3s^3 p^6 4s^2$ for Ca. The energy cutoff for the plane wave was 700 eV for SiO_2 and somewhat lower, 500 eV, for CaSiO_3 to compare directly with previous CaSiO_3 DFT studies [20,25].

In all runs, the atoms were initially placed at their ideal crystallographic sites, i.e., the $1b$, $1a$, and $3d$ positions for Ca, Si, and O atoms, respectively, of the $Pm\bar{3}m$ space group (CaSiO_3). SiO_2 MD runs were started from the ideal cubic pyrite-type structure ($Pa\bar{3}$) optimized to target an equilibrium pressure ~ 160 GPa. This is probably slightly below the stability field of the pyrite structured SiO_2 near the melting curve [38], but in order to compare directly with results in Refs. [24,39] we use pyrite rather than seifertite. The estimated melting point when pyrite is used as the crystal structure is only slightly lower compared to that found using seifertite [24,39]. For CaSiO_3 we use a cubic 135-atom simulation box which is the same as that used in previous computational studies of CaSiO_3 melting [20,25] allowing for a direct comparison with these studies. For SiO_2 , the simulation box contained 96 atoms.

Melting simulations are carried out in the NVE ensemble with a time step of 0.5 fs for SiO_2 and 1 ps for CaSiO_3 . The smaller time step for SiO_2 was chosen to minimize the energy fluctuation. All runs used in the waiting time analysis were carried out until melting plus an additional 5–20 ps to calculate the average liquid temperature.

The waiting-time analysis was performed based on between 8 and 20 different simulations at a given (E, V) where, in each run, the initial velocities were taken from a Maxwell-Boltzmann distribution. Close to the equilibrium melting temperature we performed typically around 20 MD runs at a given (E, V) to ensure that sufficient statistics were collected in order to calculate T_m using Eq. (3). Plots of the convergence of the estimated melting temperature with number of configurations are shown in the Supplemental Material [53]. This analysis shows that about 8–10 MD runs, for a given initial temperature, are sufficient to converge the melting temperature to less than 100 K. All MD calculations launched below E_h lasted for at least 10 ps and close to T_h the MD simulations typically ran for more than 100 ps.

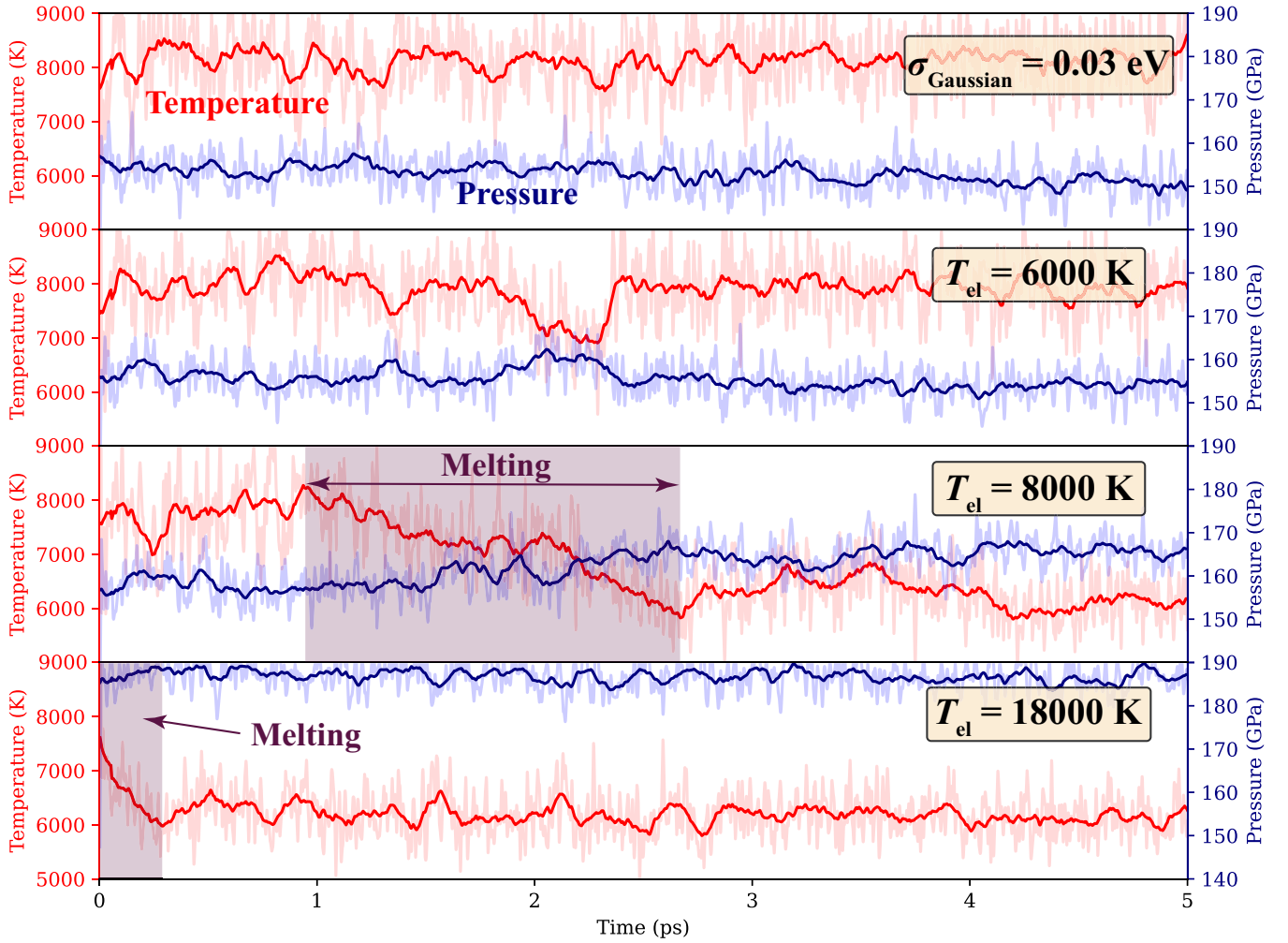


FIG. 1. Temperature (red) and pressure (blue) evolutions along *ab initio* MD trajectories for SiO₂ with different T_{el} . The thin lines show dumps every time step whereas the thick lines are averaged properties over the previous 100 time steps. All MD runs are carried out with the same initial temperature ($T_{ini} = 18000$ K) where the atoms are distributed at their equilibrium lattice positions before we launch the MD run. A Gaussian smearing broadening scheme with $\sigma_{\text{Gaussian}} = 0.03$ eV is used to represent simulations with a negligible contribution to electronic entropy on the ionic dynamics. The shaded areas show the melting process.

For SiO₂, the T_{el} are 6000, 7000, and 8000 K where 6000 K is expected, after test calculations, to lie close to T_m whereas 8000 K will lie close to T_h . Similarly, for CaSiO₃ the waiting-time analysis was carried out at $T_{el} = 6500$ and 9000 K which are expected to be close to T_m and T_h , respectively. To simulate melting with negligible contribution from the electronic entropy we used a Gaussian scheme [33] with a very low value of the smearing parameter (i.e., $\sigma_{\text{Gaussian}} = 0.03$ eV). The Gaussian smearing method is better designed to avoid instabilities arising from fluctuations in orbital occupancies at low values of σ (low temperatures) which often hamper the Fermi-Dirac method during energy minimizations. The Gaussian smearing has the functional form $\frac{1}{2}(1 - \text{erf}(\frac{\epsilon - \mu}{\sigma}))$ and the link between the two schemes is given by the ratios of the full width at half-maximum (FWHM) as

$$\frac{\text{FWHM}_{\text{Fermi-Dirac}}}{\text{FWHM}_{\text{Gaussian}}} = \frac{\cosh^{-1}(\sqrt{2})}{\sqrt{\ln 2}}. \quad (8)$$

IV. RESULTS AND DISCUSSION

A. Influence of electronic entropy on ionic dynamics

In Fig. 1 we illustrate the sensitivity to changes in electronic temperature on the melting dynamics for silica where the initial ionic temperatures are *the same* in all runs. In the extreme case where the electronic temperature is the same as the initial temperature in the MD runs ($T_{el} = T_{ini} = 18000$ K), SiO₂ always melts rapidly and instantaneously in less than 0.5 ps. On the contrary, in runs with negligible contribution from electronic entropy (i.e., with $\sigma_{\text{Gaussian}} = 0.03$ eV), melting is rare and we observed only one incidence of melt nucleation in all our 20 runs which lasted 10 ps each.

In simulations with “intermediate” T_{el} , close to either the homogeneous or the equilibrium melting temperatures (i.e., with $T_{el} = 8000$ K or $T_{el} = 6000$ K, respectively), the system with $T_{el} = 6000$ K melted markedly slower compared to those with $T_{el} = 8000$ K and the waiting time was much longer. We found that the average waiting time was 2.7 ps when $T_{el} = 8000$ K $\approx T_h$ and markedly longer by a factor

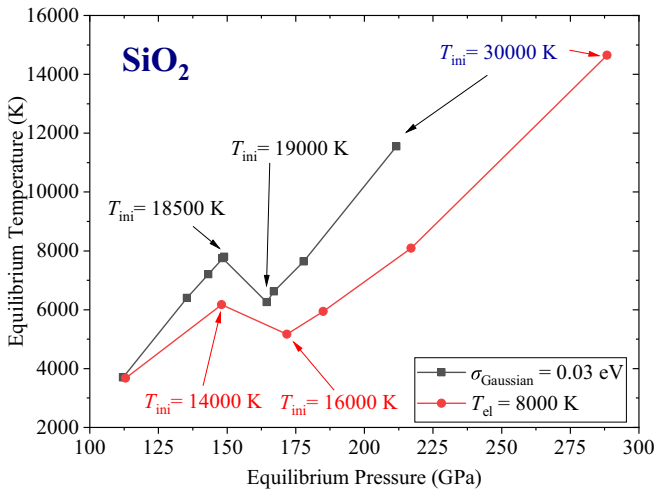


FIG. 2. Two isochores with different electronic temperatures. The black curve is runs where $\sigma_{\text{Gaussian}} = 0.03$ eV and the red curve is runs where $T_{\text{el}} = 8000 \approx T_m$. The initial temperatures are in the range 8000 to 30 000 K with the ions initially placed at their ideal lattice positions before we launched the MD simulations which ran for 20 ps each.

of about 3 when $T_{\text{el}} = 6000 \approx T_m$. See also the discussion about distributions of the waiting time in the Supplemental Material [53]. Interestingly, when $T_{\text{el}} = 6000$ K, we observe that the temperature sometimes drops markedly indicating possibly the formation of melt nuclei, but the system quickly reverted to its original (solid) state. This is seen as small “bumps” in the temperature and pressure evolutions in Fig. 1 at about 2.0–2.5 ps. Solid-liquid “oscillations” are often seen in runs where the energy is close to the target homogeneous melting energy using small simulation boxes with large temperature fluctuations [23] and will be discussed more in the Supplemental Material [53].

The influence of electronic entropy on properties is also seen in Fig. 2 where two isochores with different electronic temperatures are drawn. Here, the initial ionic temperature in the MD runs is systematically increased from 8000 to 30 000 K. The isochore with an high electronic temperature, i.e., close to T_h (i.e., with $T_{\text{el}} = 8000$ K) deviates strongly from the one with negligible contributions from electronic entropy (i.e., $\sigma_{\text{Gaussian}} = 0.03$ eV).

B. Choice of electronic temperature in *ab initio* MD runs

The sensitivity in melting temperature to choice of T_{el} illustrated above for SiO_2 and discussed in the Supplemental Material [53] suggests that BOMD runs in the NVE ensemble – where the ions are propagated using the Hellmann-Feynman forces with $\Omega + K$ being conserved – may introduce some errors due to changes in electron-ion interactions following large drops in temperature $\approx (\ln 2)/3 \times T_m$. This is seen in the Z plots and the waiting-time analysis in Figs. 3 and 4 as well as in Table I for both SiO_2 and CaSiO_3 . When T_{el} is kept fixed at some value near T_m , the calculated equilibrium melting temperature will be markedly higher compared to that if T_{el} is close to the homogeneous melting temperature. The calculated melting temperatures with $T_{\text{el}} \approx T_m$ at around 100 GPa (CaSiO_3) and 150 GPa (SiO_2) are about 300 and 200 K higher, respectively, than those calculated with $T_{\text{el}} \approx T_h$. This corresponds roughly to 10% of the temperature drop accompanying melting. We expect that these absolute errors increase with increasing melting temperature and pressure since the temperature drop accompanying melting increases with increasing T_h .

A key question is therefore as follows: What is the best choice of electronic temperature in the MD runs to minimize the errors in the calculated T_m when the ions are propagated using Hellmann-Feynmann forces with $\Omega + K$ being conserved? If we choose an electronic temperature very close

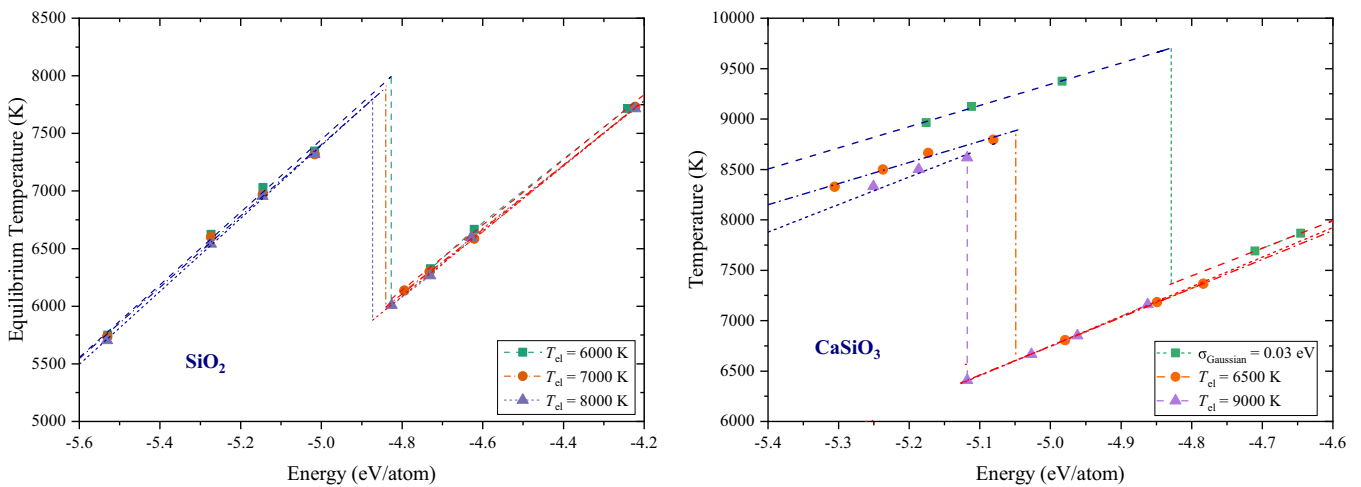


FIG. 3. Solid (blue) and liquid (red) branches in MD-NVE runs for SiO_2 (left) and CaSiO_3 (right). For SiO_2 , $T_{\text{el}} = 6000, 7000,$ and 8000 K whereas for CaSiO_3 , T_{el} are 6500 and 9000 K. In addition, we plot the result for CaSiO_3 with a Gaussian smearing scheme using $\sigma_{\text{Gaussian}} = 0.03$ eV. The homogeneous melting temperatures are calculated from an intersection of a linear extrapolation of the solid branch runs and a vertical line drawn from the equilibrium melting point [calculated using Eq. (3)]. The resulting homogeneous melting temperatures may therefore represent an upper bound to the “true” homogeneous melting temperature since the slope of the solid branch typically decreases near T_h [22,25]. Values of T_h are reported in Table I.

TABLE I. Calculated melting temperatures for CaSiO_3 and SiO_2 using the Z method together with previous values reported in the literature at similar pressure (i.e., about 103 GPa for CaSiO_3 and 160 GPa for SiO_2). In the simulation where $T_{\text{el}} \sim 0$ we used a Gaussian smearing, $\sigma_{\text{Gaussian}} = 0.03$ eV, for the partial occupancies of the one-electron orbitals. In the simulation from Ref. [25] where T_{el} is labeled as “adjust^b”, the Fermi-Dirac smearing was updated about every 1 ps along the MD trajectory to match the average temperature in the previous ~ 1 ps, as discussed in Ref. [25]. In “adjust^a” we update the electronic entropy only once along the MD trajectory after about 25 ps of propagation in the liquid state.

System	Method	T_{el} (K)	P (GPa)	T_h (K)	T_m (K)	Ref.
CaSiO_3	Z Method	9000	103.7 ± 2.6	8873 ± 42	6410 ± 21	This work
	Z Method	6500	103.0 ± 2.5	8652 ± 25	6647 ± 49	This work
	Z Method	~ 0	105.2 ± 3.0	9605 ± 11	7258 ± 38	This work
	Z Method	adjust ^a	102.6 ± 2.7	8506	6517	This work
	Z Method	adjust ^b	105 ± 3.3	8806	6493	Hernandez <i>et al.</i> [25]
	Z Method	Not reported	103.0 ± 0.2	7120	5200	Braithwaite and Stixrude [20]
	Large-size coexistence		≈ 103		6582	Hernandez <i>et al.</i> [25]
	Thermodynamic integration		≈ 103		6433	Hernandez <i>et al.</i> [25]
Two-phase thermodynamics		≈ 103		5420	Hernandez <i>et al.</i> [25]	
SiO_2	Z Method	6000	164 ± 4.3	8058 ± 39	6110 ± 60	This work
	Z Method	7000	164 ± 4.3	7899 ± 30	6015 ± 35	This work
	Z Method	8000	166 ± 4.3	7789 ± 17	5884 ± 21	This work
	Z Method	adjust ^a	169 ± 4.3		6044	This work
	Coexist		153.8		5990	Benlonoshko <i>et al.</i> [57]
	Coexist		157.6		5986	Usui <i>et al.</i> [58]
	Shock experiment		157.0		5543	Millot <i>et al.</i> [59]
	Z Method	Not reported	132.3		5852	González-Cataldo <i>et al.</i> [39]
	DAC experiment		117		≈ 6200	Andraut <i>et al.</i> [60]

to T_h in MD runs with $E = E_h$, the electronic temperature is very close to the (ensemble) average temperature before the system eventually melts. Runs with $T_{\text{el}} \approx T_h$ therefore enable the accurate calculation of T_h as well as the waiting time and imply that MD runs where $T_{\text{el}} < T_h$ (if, say $T_{\text{el}} = T_m$) give too high homogeneous melting temperatures.

Although $T_{\text{el}} \approx T_h$ (with $E \approx E_h$) enables the accurate calculation of T_h , the melting temperature may be severely

underestimated. This is because T_{el} is much larger than the liquid (ionic) temperature which, in general, favors an entropic stabilization of the liquid over the solid and hence the calculated melting temperature will be too low. If we rather chose $T_{\text{el}} \approx T_m$, which is the lowest temperature on the isochore and therefore represents a reasonable lower bound to choice of T_{el} , the homogeneous melting temperature and possibly the equilibrium melting temperature will be

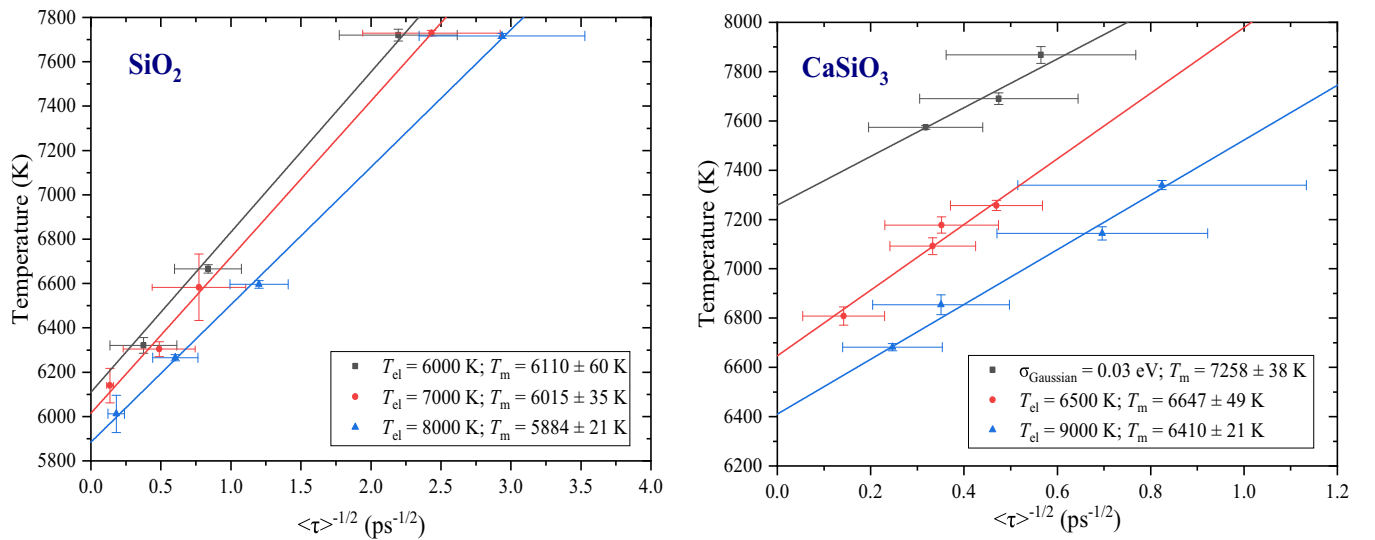


FIG. 4. The calculated melting temperature using Eq. (3) for different choices of electronic temperatures. For SiO_2 , $T_{\text{el}} = 6000, 7000,$ and 8000 K whereas for CaSiO_3 , T_{el} are 6500 and 9000 K. In addition, calculate the melting temperature using Eq. (3) for CaSiO_3 using a Gaussian smearing scheme with $\sigma_{\text{Gaussian}} = 0.03$ eV. The resulting estimated equilibrium melting temperatures are reported in Table I along with the standard error. The horizontal and vertical error bars reported are the mean errors of the waiting time and temperatures, respectively.

overestimated. Calculations where T_{el} is chosen to target either T_m or T_h , therefore, provide reasonable *upper and lower bounds*, respectively, to the true melting temperature.

C. CaSiO₃ melting

As shown in Table I, our melting temperatures are in very good agreement with a previous Z method study [25] and also in excellent agreement with those from thermodynamic integration and two-phase calculations [25]. The inclusion of electronic entropy is essential for the accurate calculation of melting temperature for CaSiO₃, in agreement with that found for other insulators such as MgO [56]. That is, the calculated T_h and T_m without contribution from the electronic entropy are about 1000 and 650 K higher, respectively, than those calculated using $T_{el} = 6500$ K. We find that the melting temperature is around 6300 K (with $T_{el} = 9000$ K) and 6600 K (with $T_{el} = 6500$ K). As discussed above, the discrepancy between the calculated melting temperature using $T_{el} = 6500$ K with that calculated using $T_{el} = 9000$ K is non-negligible for the accurate calculation of melting temperature. This places some constraints on the accuracy of the Z method interfaced with BOMD where $\Omega + K$ is conserved and the ions are propagated using Hellmann-Feynman forces in the NVE ensemble.

Choice of electronic entropy could therefore possibly explain the large discrepancy of more than 1000 K between our melting point and that of a recent Z method study [20] which was carried out at the same thermodynamic conditions as here. We use the same exchange-correlation functional to DFT as that employed in Ref. [20], but are unable to reproduce their melting point unless we set $T_{el} = T_{ini}$. Reference [20], however, does not report values of T_{el} , so no firm conclusions can be drawn.

D. SiO₂ melting

There are not many experimental studies of SiO₂ that report melting temperatures to very high pressure. Results from a recent high-pressure experimental study [59] was fitted to an equilibrium melting curve to about 500 GPa [$T_m(P) = 1968.5 + 307.8 \times P^{0.485}$] suggesting that SiO₂ melts at around 5540 K at 157 GPa. This is slightly lower than that calculated from a Z method simulation [39], where the melting temperature was estimated to be 5850 K at 132 GPa. By contrast, a recent Diamond Anvil Cell (DAC) experimental study [60,61] suggests a markedly higher melting curve compared to those mentioned above and the Clapeyron slope is also much steeper in the pressure region 120–150 GPa compared to that reported by, e.g., Millot *et al* [59]. The melting curves from two molecular dynamics simulations [57,58] using two-phase coexisting methods are in overall good agreement with that from the DAC study [60,61], but without the rapid change in the Clapeyron slope seen in the DAC experiment at around 120 GPa.

Our calculated melting temperatures reported in Table I are in overall good agreement with previous computational predictions at similar pressures [57,58]. The calculated melting temperature reported using $T_{el} = 8000$ K, for example, is 5776 K. This is only slightly lower compared to those of Refs. [57,58] which are 5990 and 5986 K, respectively. Of

note is that the good agreement with that reported by Usui and Tschuchia [58] may be fortuitous because a very small two-phase simulation box containing only 48 atoms for each phase was used in Ref. [58]. Such a small box has a boundary that is of similar size as the solid and liquid portions, and many runs are needed at a given (E, V) to precisely determine the melting points [62]. Our result also suggests that the predicted equilibrium melting curve reported from a shock experiment study [59] may be too low since it is assumed that stishovite is able to crystallize at the timescale of the experiment and the melting curve is therefore drawn at the bottom of the liquid branch of the Hugoniot. If, however, stishovite is unable to crystallize at the timescale of the shock experiment (i.e., within a few nanoseconds), the melting temperature reported in Ref. [59] may be underestimated as suggested in Ref. [63]. This interpretation is consistent with our calculated melting point.

As discussed above, the calculated melting temperature using $T_{el} = 8000$ K is slightly less than 200 K lower than that calculated using $T_{el} = 6000$ K. This difference in the calculated melting temperature is of similar size compared to that found for CaSiO₃ at similar conditions and confirms that the Z method may be hampered by some artificial features for the accurate calculations of melting temperature with the Mermin free energy + ionic kinetic energy being conserved along the Born-Oppenheimer MD-NVE trajectory with T_{el} kept fixed.

E. Sensitivity to changes in electronic entropy on the waiting-time analysis

The waiting time for the solid to melt is correctly described if we chose $T_{el} \approx \langle T \rangle_{sol}$ after equilibration (i.e., if, for example, $T_{el} = T_h$ when $E = E_h$). However, since the melting temperature is in general underestimated with $T_{el} = T_h$, interpolation to infinite waiting time using Eq. (3) gives a too low equilibrium melting temperature when $\langle \tau \rangle$ is extrapolated to infinite waiting time. However, if we use a lower T_{el} [i.e., if we chose $T_{el} = \langle T \rangle_{liq}$] the waiting time for the system to melt will be too slow. This implies that $\langle \tau \rangle^{-1/2}$ should be shifted to lower temperatures, indicating that the melting temperature calculated from the intersection $\langle \tau \rangle^{-1/2} = 0$ will be overestimated. The estimated melting temperatures from a waiting-time analysis with $T_{el} \approx T_m$ and $T_{el} \approx T_h$, therefore, provide reasonable upper and lower bounds, respectively, to the “true” equilibrium melting temperature. These differences (~ 200 – 300 K) are much larger than the standard errors from the waiting-time analysis (reported in Table I) which, in our case, are always less than 60 K. Convergence plots of the calculated melting temperatures using Eq. (3) with number of MD runs show that only a few tens of MD calculation are needed for the accurate calculation of melting temperatures (see Supplemental Material [53]).

To further understand the role of electronic entropy on the Hellmann-Feynman dynamics we can follow a similar strategy as in Ref. [25] by adjusting the electronic temperature along the MD trajectory to match the average ionic temperature after transition to the liquid state. We thus pick one of the MD runs with $T_{el} \approx T_h$ and a total energy which is marginally higher than E_h . Using CaSiO₃ as an example,

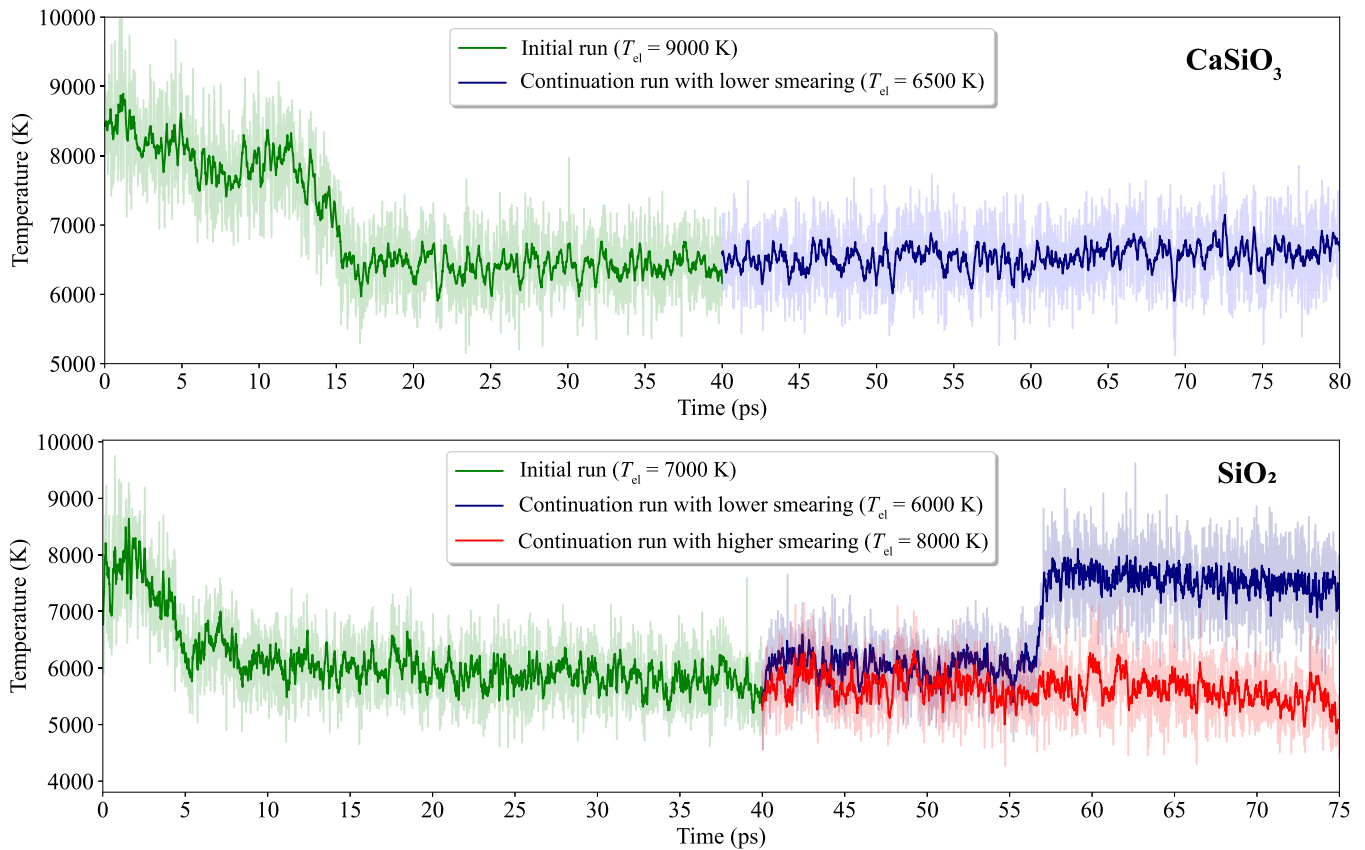


FIG. 5. Blue and red lines are continuation runs after about 40 ps of simulations (green lines). These continuation runs restarted with the same atomic positions and forces as the last step of the initial (green) run, but with different electronic temperatures. For CaSiO_3 , the MD run was initially launched with $T_{\text{el}} = 9000$ K (green line) and then restarted with $T_{\text{el}} = 6500$ K (blue line). For SiO_2 , we started with $T_{\text{el}} = 7000$ K (green line) and then continued with $T_{\text{el}} = 6000$ K (blue line) and 8000 K (red line).

we expect that the average liquid temperature is close to the equilibrium melting temperature estimated from Eq. (3). Indeed, $\langle T \rangle$ after melting is 6408 K at ~ 105 GPa, which is within the error bars of T_m (6410 ± 21 K). The simulation was then restarted after 25 ps of propagation in the liquid state with a new electronic temperature chosen to match the average liquid temperature. In Fig. 5 (top panel) we show the temperature evolution of this restarted run (blue). The total energy increased by about 1% accompanied by a temperature increase of about 100 K to 6517 K (labeled as “adjust” in Table I). The $\langle T \rangle_{\text{liq}}$ from this relaunched MD run (blue line) is higher and lower, respectively, than the melting temperature reported in Table I for $T_{\text{el}} = 9500$ and 6500 K, respectively. This confirms that Z method calculations with $T_{\text{el}} \approx T_h$ and $T_{\text{el}} \approx T_m$ represent reasonable lower and upper respectively to the true melting temperature.

Figure 5 for SiO_2 also demonstrates that changes in electronic entropy can have a substantial impact on the ionic dynamics. Here we relaunch a simulation by changing the electronic temperatures from 7000 K (green line) to $T_{\text{el}} = 6000$ K (blue line) or $T_{\text{el}} = 8000$ K (red line). Whereas the MD run with $T_{\text{el}} = 6000$ K *recrystallized* after about 15 ps of propagation in the liquid state, the simulation with $T_{\text{el}} = 8000$ K remained stable in the liquid phase until the run was terminated after more than 35 ps.

V. CONCLUSIONS

In this work, we used the Z method together with *ab initio* Born-Oppenheimer molecular dynamics to calculate the melting temperature for SiO_2 and CaSiO_3 at outer core and lower mantle conditions, respectively, with simulation boxes containing ~ 100 atoms only. The calculated melting temperature for CaSiO_3 is in excellent agreement with results from previously reported two-phase coexistence calculations and thermodynamic integration and is substantially higher than that calculated in a previous *ab initio* study using the Z method [20]. A possible explanation for this discrepancy has been discussed. The calculated melting temperature for SiO_2 is also in overall good agreement with previous computational work carried out at similar pressure and temperature suggesting that the estimated equilibrium melting curve reported in Ref. [59] may be too flat.

One of the great advantages with the Z method compared to other popular methods to melting, such as two-phase simulations and thermodynamic integration, is that the equilibrium melting temperature can be accurately calculated using small or modest-sized simulation boxes. This is because homogeneous melting is in general triggered by the formation of defects and small liquid clusters which can be embedded in a fairly small simulation box [22]. Moreover, since the melting temperature is obtained from the relationship between T_h and

T_m using Eq. (1), the Z method avoids the calculation of free energies which can be extremely tedious and expensive. The Z method can easily be implemented and interfaced with popular *ab initio* simulation software such as VASP [45,46] and is embarrassingly parallelizable.

In spite of many appealing advantages compared to other methods to melting, the Z method appears to be hampered by some artificial features which need to be much better addressed. One of these, investigated here, is the choice of electronic entropy in Born-Oppenheimer MD simulation carried out in the microcanonical ensemble when $K + \Omega$ is a conserved and hence T_{el} is kept fixed along the Hellmann-Feynman trajectory. Since melting is accompanied by a large drop in temperature we need to quantify the errors introduced due to the choice of electronic temperature. We, therefore, compare the melting temperatures calculated using $T_{el} \approx T_h$ and $T_{el} \approx T_m$ since these two electronic temperatures give reasonable lower and upper bounds to the true melting temperature. For SiO₂ and CaSiO₃ at high pressure and temperature, the difference in the calculated T_m with $T_{el} \approx T_h$ and $T_{el} \approx T_m$ is about 200–300 K. Although these discrepancies are only a few percent of the melting temperature, they are in general not negligible for the accurate calculation of

melting temperature and are important to take into account for a critical assessment of the Z method implemented together with Born-Oppenheimer MD in the NVE ensemble where the ions are propagated using Hellmann-Feynman forces with a fixed electronic temperature. If the adiabatic approximation is valid, the ions can, in theory, be propagated using the force given by Eq. (5); but if the adiabatic approximation breaks down, the correct dynamics is governed by conservation laws derived from, e.g., Ehrenfest dynamics using the all-electron time-dependent Kohn-Sham or Schrödinger equations.

ACKNOWLEDGMENTS

We thank Prof. D. Alfè for the thoughtful discussion. The Centre for Earth Evolution and Dynamics is funded by the Research Council of Norway through its Centre of Excellence program (Grant No. 223272). We acknowledge financial support from the Research Council of Norway through its Centres of Excellence scheme, Project No. 332523 (PHAB). Computational resources were provided by the Norwegian infrastructure for high-performance computing (NOTUR, Sigma-2, Grants No. NN9329K and No. NN2916K).

-
- [1] A. B. Belonoshko, N. V. Skorodumova, A. Rosengren, and B. Johansson, Melting and critical superheating, *Phys. Rev. B* **73**, 012201 (2006).
- [2] V. Olguin-Arias, S. Davis, and G. Gutiérrez, Extended correlations in the critical superheated solid, *J. Chem. Phys.* **151**, 064507 (2019).
- [3] C. J. Rossouw and S. E. Donnelly, Superheating of small solid-argon bubbles in aluminum, *Phys. Rev. Lett.* **55**, 2960 (1985).
- [4] J. B. Boyce and M. Stutzmann, Orientational ordering and melting of molecular H₂ in an *a*-Si matrix: NMR studies, *Phys. Rev. Lett.* **54**, 562 (1985).
- [5] R. W. Cahn, Materials science: Melting and the surface, *Nature (London)* **323**, 668 (1986).
- [6] J. H. Evans and D. J. Mazey, Solid bubble formation in titanium injected with krypton ions, *J. Nucl. Mater.* **138**, 176 (1986).
- [7] M. Z. Mo, Z. Chen, R. K. Li, M. Dunning, B. B. L. Witte, J. K. Baldwin, L. B. Fletcher, J. B. Kim, A. Ng, R. Redmer, A. H. Reid, P. Shekhar, X. Z. Shen, M. Shen, K. Sokolowski-Tinten, Y. Y. Tsui, Y. Q. Wang, Q. Zheng, X. J. Wang, and S. H. Glenzer, Heterogeneous to homogeneous melting transition visualized with ultrafast electron diffraction, *Science* **360**, 1451 (2018).
- [8] G. Zhang, X. Fan, Q. Zhang, Q. Li, Y. Wu, and M. Li, Partial disordering and homogeneous melting in multicomponent systems, *Acta Mater.* **239**, 118281 (2022).
- [9] A. R. Finney and P. M. Rodger, Applying the Z method to estimate temperatures of melting in structure II clathrate hydrates, *Phys. Chem. Chem. Phys.* **13**, 19979 (2011).
- [10] B. K. Benazzouz, A. Zaoui, and A. B. Belonoshko, Determination of the melting temperature of kaolinite by means of the Z-method, *Am. Mineral.* **98**, 1881 (2013).
- [11] F. Saiz, An *ab initio* study on liquid silicon carbide, *J. Phys. Chem. Solids* **137**, 109204 (2020).
- [12] S. R. Baty, L. Burakovsky, and D. Errandonea, *Ab initio* phase diagram of silver, *J. Phys.: Condens. Matter* **33**, 485901 (2021).
- [13] A. B. Belonoshko, L. Burakovsky, S. P. Chen, B. Johansson, A. S. Mikhaylushkin, D. L. Preston, S. I. Simak, and D. C. Swift, Molybdenum at high pressure and temperature: Melting from another solid phase, *Phys. Rev. Lett.* **100**, 135701 (2008).
- [14] J. Bouchet, F. Bottin, G. Jomard, and G. Zerah, Melting curve of aluminum up to 300 GPa obtained through *ab initio* molecular dynamics simulations, *Phys. Rev. B* **80**, 094102 (2009).
- [15] A. B. Belonoshko and A. Rosengren, High-pressure melting curve of platinum from *ab initio* Z method, *Phys. Rev. B* **85**, 174104 (2012).
- [16] H. Y. Geng, R. Hoffmann, and Q. Wu, Lattice stability and high-pressure melting mechanism of dense hydrogen up to 1.5 TPa, *Phys. Rev. B* **92**, 104103 (2015).
- [17] L. Burakovsky, N. Burakovsky, and D. L. Preston, *Ab initio* melting curve of osmium, *Phys. Rev. B* **92**, 174105 (2015).
- [18] Y. Zhang, Y. Tan, H. Y. Geng, N. P. Salke, Z. Gao, J. Li, T. Sekine, Q. Wang, E. Greenberg, V. B. Prakapenka, and J.-F. Lin, Melting curve of vanadium up to 256 GPa: Consistency between experiments and theory, *Phys. Rev. B* **102**, 214104 (2020).
- [19] D. V. Minakov, M. A. Paramonov, G. S. Demyanov, V. B. Fokin, and P. R. Levashov, *Ab initio* calculation of hafnium and zirconium melting curves via the Lindemann criterion, *Phys. Rev. B* **106**, 214105 (2022).
- [20] J. Braithwaite and L. Stixrude, Melting of CaSiO₃ perovskite at high pressure, *Geophys. Res. Lett.* **46**, 2037 (2019).
- [21] S. M. Stishov, I. N. Makarenko, V. A. Ivanov, and A. M. Nikolaenko, On the entropy of melting, *Phys. Lett. A* **45**, 18 (1973).
- [22] S. Davis, S. Loyola, and J. Peralta, Bayesian statistical modeling of microcanonical melting times at the superheated regime, *Phys. A (Amsterdam)* **515**, 546 (2019).

- [23] D. Alfé, C. Cazorla, and M. J. Gillan, The kinetics of homogeneous melting beyond the limit of superheating, *J. Chem. Phys.* **135**, 024102 (2011).
- [24] F. González-Cataldo, S. Davis, and G. Gutierrez, Z method calculations to determine the melting curve of silica at high pressures, *J. Phys.: Conf. Ser.* **720**, 012032 (2016).
- [25] J.-A. Hernandez, C. E. Mohn, M. G. Guren, M. A. Baron, and R. G. Trønnes, *Ab initio* atomistic simulations of Ca-perovskite melting, *Geophys. Res. Lett.* **49**, e2021GL097262 (2022).
- [26] C. Di Paola and J. P. Brodholt, Modeling the melting of multicomponent systems: The case of MgSiO₃ perovskite under lower mantle conditions, *Sci. Rep.* **6**, 29830 (2016).
- [27] B. Grabowski, L. Ismer, T. Hickel, and J. Neugebauer, *Ab initio* up to the melting point: Anharmonicity and vacancies in aluminum, *Phys. Rev. B* **79**, 134106 (2009).
- [28] A. I. Duff, T. Davey, D. Korbacher, A. Glensk, B. Grabowski, J. Neugebauer, and M. W. Finnis, Improved method of calculating *ab initio* high-temperature thermodynamic properties with application to ZrC, *Phys. Rev. B* **91**, 214311 (2015).
- [29] S.-T. Lin, M. Blanco, and W. A. Goddard, The two-phase model for calculating thermodynamic properties of liquids from molecular dynamics: Validation for the phase diagram of lennard-jones fluids, *J. Chem. Phys.* **119**, 11792 (2003).
- [30] L.-F. Zhu, B. Grabowski, and J. Neugebauer, Efficient approach to compute melting properties fully from *ab initio* with application to Cu, *Phys. Rev. B* **96**, 224202 (2017).
- [31] S. Wang, G. Zhang, H. Liu, and H. Song, Modified z method to calculate melting curve by molecular dynamics, *J. Chem. Phys.* **138**, 134101 (2013).
- [32] A. V. Karavaev, V. V. Dremov, and T. A. Pravishkina, Precise calculation of melting curves by molecular dynamics, *Comput. Mater. Sci.* **124**, 335 (2016).
- [33] A. de Vita, The energetics of defects and impurities in metal and ionic materials from first principles, Ph.D. thesis, Keele University, 1992.
- [34] R. M. Wentzcovitch, J. L. Martins, and P. B. Allen, Energy versus free-energy conservation in first-principles molecular dynamics, *Phys. Rev. B* **45**, 11372 (1992).
- [35] M. Weinert and J. W. Davenport, Fractional occupations and density-functional energies and forces, *Phys. Rev. B* **45**, 13709 (1992).
- [36] A. Corgne, C. Liebske, B. J. Wood, D. C. Rubie, and D. J. Frost, Silicate perovskite-melt partitioning of trace elements and geochemical signature of a deep perovskitic reservoir, *Geochim. Cosmochim. Acta* **69**, 485 (2005).
- [37] S. Tateno, K. Hirose, S. Sakata, K. Yonemitsu, H. Ozawa, T. Hirata, N. Hirao, and Y. Ohishi, Melting phase relations and element partitioning in morb to lowermost mantle conditions, *J. Geophys. Res.: Solid Earth* **123**, 5515 (2018).
- [38] P. K. Das, C. E. Mohn, J. P. Brodholt, and R. G. Trønnes, High-pressure silica phase transitions: Implications for deep mantle dynamics and silica crystallization in the protocore, *Am. Mineral.* **105**, 1014 (2020).
- [39] F. González-Cataldo, S. Davis, and G. Gutierrez, Melting curve of SiO₂ at multimegabar pressures: Implications for gas giants and super-earths, *Sci. Rep.* **6**, 26537 (2016).
- [40] K. Hirose, Crystallization of silicon dioxide and compositional evolution of the earth's core, *Nature (London)* **543**, 99 (2017).
- [41] R. G. Trønnes, M. A. Baron, K. R. Eigenmann, M. G. Guren, B. H. Heyn, A. Løken, and C. E. Mohn, Core formation, mantle differentiation and core-mantle interaction within earth and the terrestrial planets, *Tectonophysics* **760**, 165 (2019).
- [42] N. D. Mermin, Thermal properties of the inhomogeneous electron gas, *Phys. Rev.* **137**, A1441 (1965).
- [43] M. R. Pederson and K. A. Jackson, Pseudoenergies for simulations on metallic systems, *Phys. Rev. B* **43**, 7312 (1991).
- [44] A. Ojanperä, V. Havu, L. Lehtovaara, and M. Puska, Nonadiabatic Ehrenfest molecular dynamics within the projector augmented-wave method, *J. Chem. Phys.* **136**, 144103 (2012).
- [45] G. Kresse and J. Hafner, *Ab initio* molecular dynamics for liquid metals, *Phys. Rev. B* **47**, 558 (1993).
- [46] G. Kresse and J. Hafner, *Ab initio* molecular-dynamics simulation of the liquid-metal-amorphous-semiconductor transition in germanium, *Phys. Rev. B* **49**, 14251 (1994).
- [47] G. Kresse and J. Furthmüller, Efficient iterative schemes for *ab initio* total-energy calculations using a plane-wave basis set, *Phys. Rev. B* **54**, 11169 (1996).
- [48] G. Kresse and J. Furthmüller, Efficiency of *ab-initio* total energy calculations for metals and semiconductors using a plane-wave basis set, *Comput. Mater. Sci.* **6**, 15 (1996).
- [49] P. E. Blöchl, Projector augmented-wave method, *Phys. Rev. B* **50**, 17953 (1994).
- [50] G. Kresse and D. Joubert, From ultrasoft pseudopotentials to the projector augmented-wave method, *Phys. Rev. B* **59**, 1758 (1999).
- [51] J. P. Perdew, K. Burke, and M. Ernzerhof, Generalized gradient approximation made simple, *Phys. Rev. Lett.* **77**, 3865 (1996).
- [52] R. Armiento and A. E. Mattsson, Functional designed to include surface effects in self-consistent density functional theory, *Phys. Rev. B* **72**, 085108 (2005).
- [53] See Supplemental Material at <http://link.aps.org/supplemental/10.1103/PhysRevB.108.134110> for Figures S1 and S2 show the convergence of T_m with the number of MD runs for both our testing systems, which includes Refs. [54,55].
- [54] C. E. Mohn, S. Stølen, and S. Hull, Diffusion within α -CuI studied using *ab initio* molecular dynamics simulations, *J. Phys.: Condens. Matter* **21**, 335403 (2009).
- [55] C. E. Mohn, S. Stølen, S. T. Norberg, and S. Hull, *Ab initio* molecular dynamics simulations of oxide-ion disorder in the δ -Bi₂O₃, *Phys. Rev. B* **80**, 024205 (2009).
- [56] D. Alfé, Melting curve of MgO from first-principles simulations, *Phys. Rev. Lett.* **94**, 235701 (2005).
- [57] A. B. Belonoshko and L. S. Dubrovinsky, Molecular dynamics of stishovite melting, *Geochim. Cosmochim. Acta* **59**, 1883 (1995).
- [58] Y. Usui and T. Tsuchiya, *Ab initio* two-phase molecular dynamics on the melting curve of SiO₂, *J. Earth Sci.* **21**, 801 (2010).
- [59] M. Millot, N. Dubrovinskaia, A. Černok, S. Blaha, L. Dubrovinsky, D. G. Braun, P. M. Celliers, G. W. Collins, J. H. Eggert, and R. Jeanloz, Shock compression of stishovite and melting of silica at planetary interior conditions, *Science* **347**, 418 (2015).

- [60] D. Andrault, L. Pison, G. Morard, G. Garbarino, M. Mezouar, M. A. Bouhifd, and T. Kawamoto, Comment on: Melting behavior of SiO₂ up to 120 GPa (andrault *et al.* 2020), *Phys. Chem. Miner.* **49**, 3 (2022).
- [61] D. Andrault, G. Morard, G. Garbarino, M. Mezouar, M. A. Bouhifd, and T. Kawamoto, Melting behavior of SiO₂ up to 120 GPa, *Phys. Chem. Miner.* **47**, 10 (2020).
- [62] Q.-J. Hong and A. van de Walle, A user guide for sluschi: Solid and liquid in ultra small coexistence with hovering interfaces, *Calphad* **52**, 88 (2016).
- [63] Y. Shen, S. B. Jester, T. Qi, and E. J. Reed, Nanosecond homogeneous nucleation and crystal growth in shock-compressed SiO₂, *Nat. Mater.* **15**, 60 (2016).